NANO LETTERS

Letter

pubs.acs.org/NanoLett

Chromatic Plasmonic Polarizers for Active Visible Color Filtering and Polarimetry

Tal Ellenbogen,* Kwanyong Seo, and Kenneth B. Crozier*

School of Engineering and Applied Sciences, Harvard University, 33 Oxford Street, Cambridge, Massachusetts 02138, United States

Supporting Information

ABSTRACT: Color filters are widely used in color displays, optical measurement devices, and imaging devices. Conventional color filters have usually only one fixed output color. However developing active color filters with controllable color output can lead to more compact and sophisticated color filter-based devices and applications. Recent progress in nanotechnology and new knowledge of the interaction of light with metal nanostructures allow us to capture and control light better than ever. Here we use it to fabricate active color filters, based on arrays of metallic optical nanoantennas that are tailored to interact with light at visible frequencies via excitation of localized surface plasmons. This interaction maps the polarization state of incident white light to visible color. Similarly, it converts unpolarized white light to chromatically polarized light. We experimentally demonstrate a wide range of applications including active color pixels, chromatically switchable and invisible tags, and polarization imaging based on these engineered colored metasurfaces.

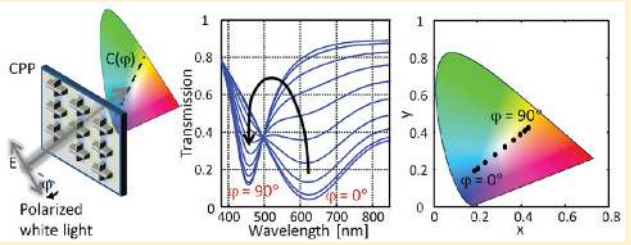

KEYWORDS: *Nano antennas, localized surface plasmons, tunable color filters, polarimetry, color pixels, plasmonic color filters*

Metal nanoparticles (MNPs) have been used for centuries to create colorful patterns in glass. One of the most famous examples is the ancient Roman Lycurgus Cup,[1] made of glass doped with MNPs, which give it a green color when viewed in reflection and a red color when viewed in transmission. The color filtering effect results from strong scattering and absorption of light by the MNP due to a resonant interaction of the electromagnetic light field at visible frequencies with free conduction electrons in the MNP. This coupled resonant electromagnetic-electron excitation is called localized surface plasmon (LSP).

At the LSP resonance, the MNP's scattering and absorption cross sections grow to several times the physical dimensions of the MNP[2] resulting in efficient filtering of specific bands of the electromagnetic spectrum.[3] Another consequence of the LSP resonance is that intensity enhancement occurs in the vicinity of the MNP.[4] This was used to enhance intensity-dependent optical phenomena, for example, optical absorption in solar cells,[2,5,6] Raman scattering,[7−11] and nonlinear optical effects.[12] The resonance frequencies of the LSPs are highly sensitive to the dielectric environment, material properties, size, and shape of the MNP.[13−15] This has enabled the use of LSPs in biological and chemical sensors.[14,16]

With recent advances in nanofabrication such as electron beam lithography and ion beam milling, we can manipulate the shape and size of MNPs and other metal nanostructures at length scales of 10 nm or below[11] and precisely control the LSP resonance. The engineered MNPs are considered as optical nanoantennas[15] (ONATs) thanks to their ability to receive optical radiation at specific frequencies and focus it at the near field, or transmit near field electromagnetic energy to the far field. The ability to shape the frequency response of metal structures[17,18] was recently employed to demonstrate impressive color filtering based on excitation of LSPs or propagating surface plasmon polaritons in different metal nanostructures, for example, periodic metal-insulator-metal nanoresonators (MIM),[19] MIM waveguides,[20] and subwavelength metal hole arrays.[21−23]

Here we present a new approach to achieve active color filtering based on specially designed plasmonic ONATs, which are termed chromatic plasmonic polarizers (CPP). While conventional color filters can be used to transmit a single color that is represented by a single point on the CIE 1931 chromaticity diagram, CPPs can produce a continuum of colors represented by a line on the chromaticity diagram where selection of the transmitted color is done by controlling the polarization of the incident light or the transmitted light. Because of the unique optical functionality of CPPs they can be used to engineer optical metamaterials with interesting applications. We experimentally demonstrate that CPPs can be used as active color pixels, for example, for color displays, as the building blocks of encrypted tags, for example, for security applications, to generate optically functionalized surfaces, and as polarization detectors, for example, for polarization microscopy and polarimetry.

The concept of CPP is illustrated in Figure 1a. CPPs are composed of arrays of metal cross structures whose vertical and

Received: December 3, 2011
Revised: December 28, 2011

 © XXXX American Chemical Society dx.doi.org/10.1021/nl204257g | *Nano Lett.* XXXX, XXX, XXX−XXX

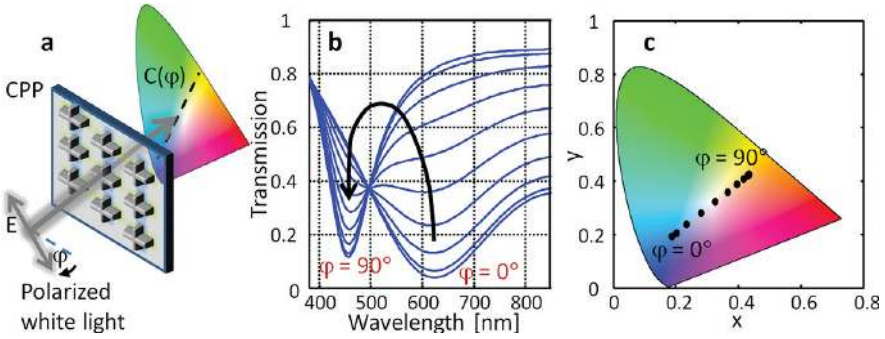

Figure 1. Conversion of polarization state to visible color by CPP. (a) Illustration of the CPP operation concept. Polarized white light is color filtered by the LSPs on the arms of the cross-shaped ONATs that comprise the CPP. The amount of filtering by each LSP is controlled by the projection of the input polarization onto it. The output color results from additive color mixing of the filtering functions of the two arms of the cross-shaped ONAT. (b) Simulated transmission spectra for linearly polarized illumination of square array of CPPs with polarization angles ranging from $\varphi = 0°$, at which yellow is blocked, to $\varphi = 90°$, at which blue is blocked, in steps of 10°. (c) Mapping of simulated transmission spectra of (b) to points on the CIE 1931 *xy* chromaticity diagram, showing active polarization-dependent blue to yellow color filtering.

horizontal arms have different lengths, being tuned to LSPs with different frequencies in the visible spectrum. The *x*- and *y*-axis periods of the array are subwavelength. When incident light is polarized along the vertical direction ($\varphi = 90°$) or along the horizontal direction ($\varphi = 0°$) with respect to the CPP orientation, dips in the transmission spectrum occur, corresponding excitation of the vertical LSP or horizontal LSP, respectively. At tilted polarization, it gives a linear superposition of the two color filters according to the projection of the polarization on the two ONATs. Thereby the polarization dependent transmission through CPPs can be represented by

$$T(\varphi, \lambda) = T_V(\lambda)\sin^2\varphi + T_H(\lambda)\cos^2\varphi \quad (1)$$

where φ is the polarization angle, λ is the free space wavelength of light, $T_V(\lambda)$ and $T_H(\lambda)$ are the transmissions for light polarized along the vertical and horizontal axes, respectively, and $T(\varphi,\lambda)$ is the wavelength and polarization-angle dependent transmission through the CPP.

To calculate the polarization-dependent transmission through CPPs, we performed finite difference time domain electromagnetic simulations (Lumerical FDTD). Figure 1b depicts the simulation results for transmission through a square array of aluminum CPPs with a period of 250 nm. Each cross has dimensions of $l_V = 120$ nm, $w_V = 40$ nm, $l_H = 200$ nm, and $w_H = 40$ nm where *l* and *w* represent the length and width, respectively, of the vertical and horizontal rods that comprise the cross ONAT, and the subscripts V and H stand for vertical and horizontal, respectively. The period of the array was kept subwavelength to avoid grating effects, as these would modify the transmission spectra. The thickness of the aluminum was 40 nm. The results are shown for polarization angles ranging from $\varphi = 0°$ to $\varphi = 90°$ in 10° steps. The two transmission dips due to the two LSPs were found at free space optical wavelengths of $\lambda_0 = 624$ nm for $\varphi = 0°$ and at $\lambda_0 = 455$ nm for $\varphi = 90°$. From these two curves, eq 1 can be used to calculate the polarization-angle dependent transmission. This was found to be in excellent agreement with the electromagnetic simulation results.

We used linear colorimetric transformations to map each polarization-angle dependent transmission spectrum to a single point in the CIE 1931 *xy* chromaticity diagram. The results are plotted as Figure 1c, demonstrating that changes in the polarization of the incident white light result in a remarkable effect on the perceived color of transmitted light. It is evident that by rotating the angle of polarization of the incident light we can produce different color outputs. The gamut of colors accessible by a single CPP is defined by a line on the CIE 1931 *xy* chromaticity diagram. The end points of the line can be determined by tuning the resonance frequency of the cross LSPs, which can be achieved by changing the shape and size of the perpendicular metal nanorods that consist the cross ONAT. Consequently, CPPs open way to design active and controllable color filters that span the entire visible spectrum and can be used for a wide variety of interesting applications.

Generation of Active Color Pixels. CPPs with different sizes and shapes were fabricated (see Supporting Information Figure S1a–f). We chose to employ aluminum as the ONAT metal because of its low price, CMOS compatibility, and high plasma frequency. The latter allows tuning the LSP resonances of the cross ONATs over the entire visible spectrum.

Figure 2 shows the results obtained from a yellow to blue CPP pixel. A scanning electron microscope image of nine representative cross ONATs is shown in Figure 2a. The period of the cross ONAT array was 250 nm with the design dimensions of each ONAT as follows: $l_H = 150$ nm, $w_H = 40$ nm, $l_V = 100$ nm, $w_V = 40$ nm, and thickness = 40 nm. To check the functionality of the CPP, we performed polarization-dependent transmission spectra measurements (see Methods). Figure 2b shows the spectral transmission results taken at polarization angles ranging from $\varphi = 0°$ to $\varphi = 90°$ in 10° steps and normalized to the transmission through bare glass slide. The LSP dips at $\varphi = 0°$ and $\varphi = 90°$ were at 620 and 460 nm, respectively. The differences between the simulation and experimental results can be explained by the high sensitivity of the LSP resonance to the material properties, size, and shape of the ONATs. It can be seen in Figure 2a (and Supporting Information Figure S1) that the fabricated ONATs suffer from some imperfections, for example, grainy aluminum deposition and broadening of the base of the cross ONATs, in addition to natural oxidation. These imperfections red shift the resonances. However we must note that when the same design parameters are used, the fabricated structures, and the optical properties they exhibit, are highly reproducible. Figure 2d shows the polarization-angle dependent transmission measured over a full 360°, demonstrating the symmetry of the CPP response around 180°. The polarization-dependent color of the CPP pixel was photographed (see Methods) and is shown in Figure 2c for the two principal polarizations of incident light. The CPP pixel shows vibrant yellow for $\varphi = 90°$ and blue for $\varphi = 0°$,

dx.doi.org/10.1021/nl204257g | *Nano Lett.* XXXX, XXX, XXX–XXX

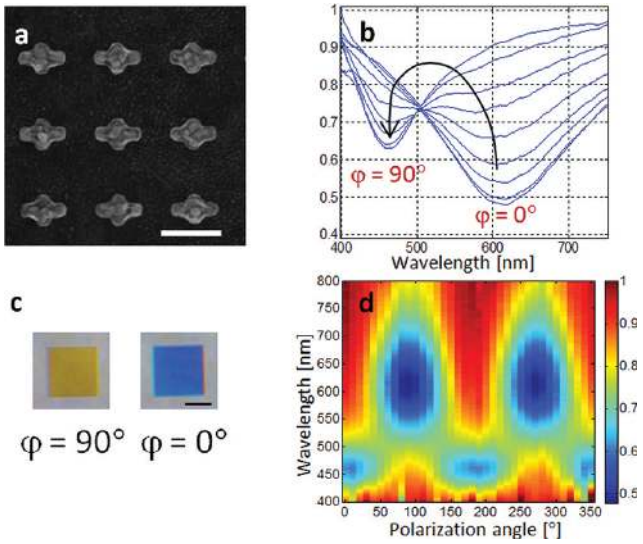

Figure 2. Experimental demonstration of yellow to blue CPP pixel. (a) SEM image of nine representative cross-shaped ONATs of the pixel. Each ONAT has arm lengths with dimensions l_H = 150 nm and l_V = 100 nm. The ONATs are arranged in a square array with period of 250 nm. The white scale bar is 200 nm long. (b) Measured polarization-angle dependent normalized transmission spectra for polarization angles varying from 0 to 90° in 10° steps. (c) Images of CPP pixel, obtained by imaging transmitted light onto color camera. Pixel appears blue when polarizer is set to 0°, while yellow for 90°. The black scale bar is 40 μm long. (d) Measured transmission vs polarization angle and wavelength.

demonstrating the large color contrast that can be obtained with a single CPP pixel. Supporting Information Movie S1 shows the continuous variation of color from yellow to blue resulting from rotation of the polarization of the incident light.

To show that CPP pixels can be designed to form different lines on the CIE 1931 *xy* chromaticity diagram, we fabricated CPP pixels with different ONAT dimensions (see Supporting Information Figure S1). We measured the transmission spectra and photographed the transmitted colors obtained when the polarizer was tuned to the principal axes of the CPPs. Figure 3

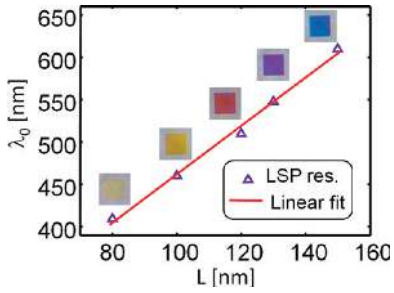

Figure 3. Tunning the color of CPPs. Measured position of transmission spectra dip vs arm length L of ONATs that comprise CPP device. Image of each ONAT array obtained by imaging transmitted light onto color camera is shown above its corresponding data point.

shows the dip position of the LSP resonance versus arm length of different cross ONATs. The small squares show photographs of the color of the CPP pixels when the light is polarized along the direction of the corresponding arm of the cross ONATs. It should be noted that the length of the other arm of the ONAT differed between ONATs. However, due to the cross shape of the ONATs, the length of the other arm is unimportant, as it is perpendicular to the arm along which the polarization is oriented and shows a negligible effect on it is LSP resonance. We measured a linear relation, λ_0 = 2.86*L+175, for the effective free space optical wavelength of the LSP, λ_0, versus the arm length, L, with agreement to the linear relation obtained with rod ONATs.[4,24] This property makes it easy to design CPPs for specific color operations.

Applications of Complex CPP Patterns. We have thus far shown results obtained with uniform CPP samples, illustrating the potential application of displays based on active pixels able to generate wide color gamut. However the concept of CPPs can be extended to create complex patterns suitable for a variety of other applications. Next we demonstrate the use of CPPs to create structures that can appear invisible, or visible with variable color, depending on polarization. These present opportunities for security tag applications. To illustrate the underlying physical mechanism, we produced a sample with CPPs forming the acronym "LSP". The array periodicity and single antenna design were similar to those used for the yellow to blue color pixel of Figure 2 with the difference that the cross ONATs in the areas composing the letters were identical to the cross ONATs in the background, but rotated 90° (Figure 4l).

Figure 4a depicts the experimental setup used to image the light transmitted through the CPP sample onto a color image sensor (see also Methods). Figure 4b–e presents transmission photographs taken for incident light that was unpolarized, 90°, 45°, and 0° polarized, respectively. It can be seen that for unpolarized light the LSP acronym is invisible and the sample shows a gray color that maps to the middle point of the CIE *xy* chromaticity diagram shown in 1(c). However, when light is polarized along one of the principal axis, a brilliant yellow and blue LSP image emerges that can be color switched by rotating the polarization of the incident light by 90°. When light is polarized at 45° to the principal axis, the tag writing is invisible again. Supporting Information Movie S2 shows the continuous variation of the appearance of the LSP tag resulting from rotation of the polarization of the incident light. Because of the uniqueness of these characteristics, these structures present the opportunity for difficult-to-reproduce security tags.

We produced another complex pattern with a square lattice of 250 nm period as before but with a $\theta(x) = 180°x/L$ rotation function of the individual CPPs where x is the spatial coordinate and L is the extent of the sample in the x direction. This results in an array of CPPs that rotate around their axes and complete a 180° rotation from one side of the sample to the other. Figure 4f–k shows the photographed transmission images of the sample obtained for incident light polarization angles of 0, 30, 60, 90, 120, and 150°. Supporting Information Movie S3 shows the continuous variation of this twisted CPP pattern as the incident light polarization is rotated. Rotating the polarization of the incident light creates a wavelike pattern of the LSPs and consequently of the transmitted color. As we describe below, this phenomenon presents an interesting opportunity for a new class of plasmonic tweezers.

The near-field hot spots created by LSPs can be used to trap micrometric and nanometric objects. It has been recently shown that, using polarization, additional manipulation capabilities are possible.[25] Wang et al.[26] demonstrated that nanoparticles can be trapped and rotated by gold nanopillars illuminated with circularly polarized light. It was shown that the hot spots rotated about the nanopillar with the optical period, and that this was accompanied by an energy flow.[26] The nanoparticles

dx.doi.org/10.1021/nl204257g | *Nano Lett.* XXXX, XXX, XXX–XXX

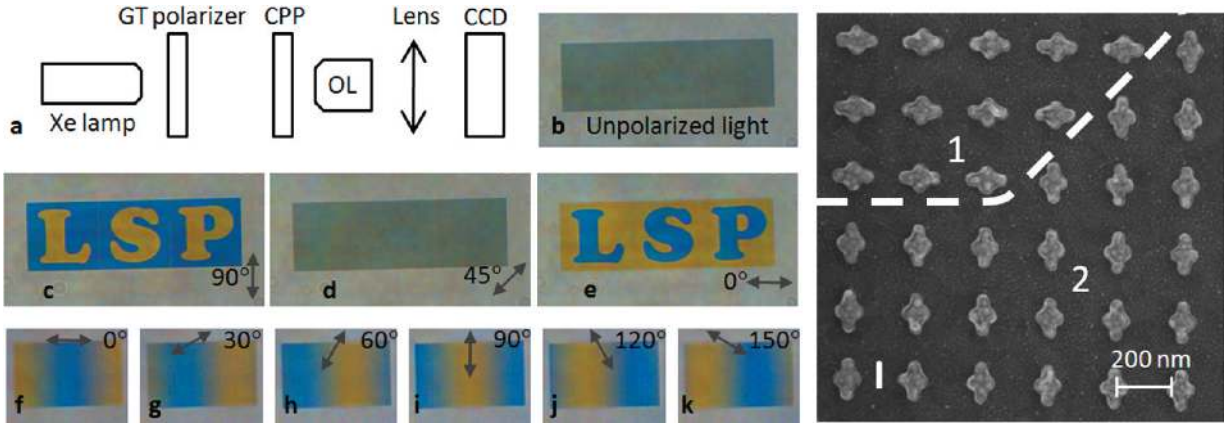

Figure 4. Demonstration of complex CPP samples. (a) Experimental setup (GT, Glan Thompson, OL, objective lens). Transmission images through LSP pattern sample for (b) unpolarized incident light, (c) 90° polarized light, (d) 45° polarized light, and (e) 0° polarized light. Transmission images through twisted CPP sample for (f) 0° polarized light, (g) 30° polarized light, (h) 60° polarized light, (i) 90° polarized light, (j) 120° polarized light, and (k) 150° polarized light. (l) SEM image of part of LSP sample showing that the background ONATs (region "2") are 90° rotated compared to the ONATs that compose the letters (region "1"). This arrangement gives the large color contrast visible in (c) and (e).

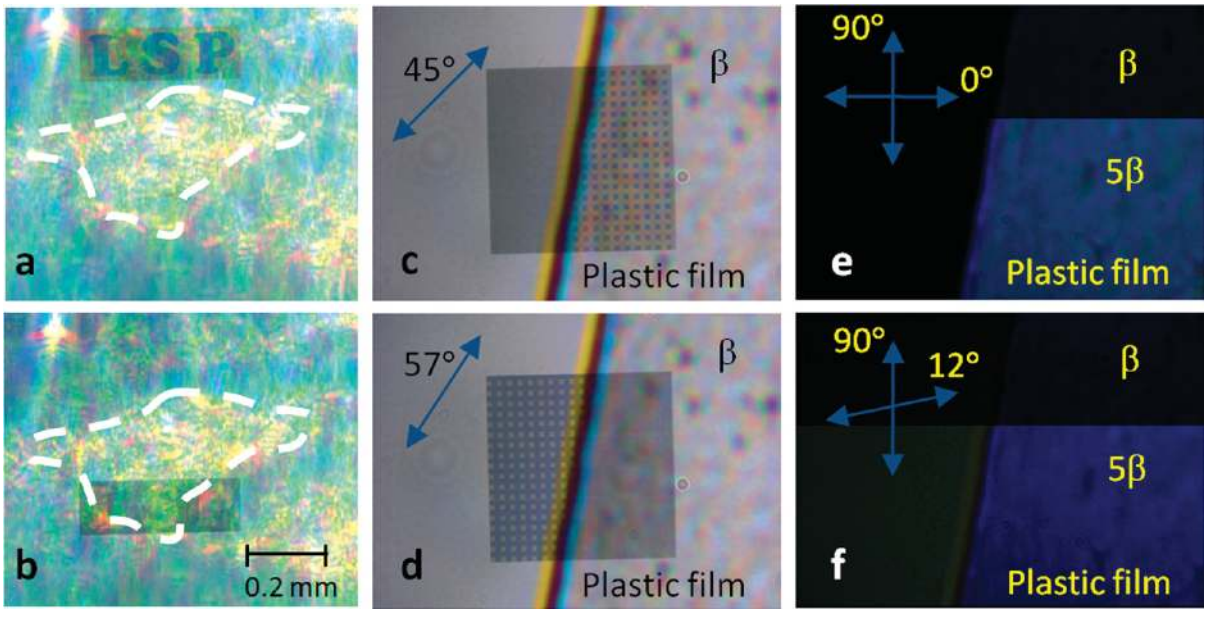

Figure 5. Polarization imaging with CPPs. (a) When imaging chicken breast tissue, the letters of CPP device appear blue, while the background appears yellow. (b) Chicken breast tissue is shifted vertically by 0.35 mm with respect to (a). CPP colors are now reversed with letters yellow and background blue, demonstrating the CPP device converts birefringence contrast to color contrast. Imaging the edge of birefringent plastic film with CPP dot pattern with input polarizer at (c) 45° and (d) 57° showing the polarization effect of the plastic film. β indicates the brightness setting level of image sensor. (e) Photograph of the plastic edge placed between two crossed polarizers. (f) Same as in (e) with input polarizer rotated by 12°.

therefore experienced a scattering force that caused them to rotate about the nanopillar. Similarly, the wavelike motion enabled by CPPs could be used to make trapped object surf on the waves of hotspots. Different shapes and trapped object transportation networks could be designed for different functionalities.

Bright-Field Polarization Imaging with CPPs. The high sensitivity of the CPP color to the incident polarization makes it suitable for use in polarization imaging applications, for example, birefringence measurements of cancerous tissues[27] or optical rotation measurements of solutions of chiral molecules. This is especially advantageous when the results are to be analyzed with the unaided eye, as is frequently done for medical images, or when viewed with a conventional color image sensor, as the CPP device maps polarization to color. We used CPP samples to perform polarization imaging of a chicken breast tissue, which is birefringent due to muscle fibers,[28] and of a birefringent plastic film. For these measurements we used complex patterns of CPP to utilize the high sensitivity of the visual cortex to color contrast.[29] We used the setup shown in Figure 4a where we added the analyzed sample between the polarizer and the CPP and imaged it on the CPP using a lens with 75 mm focal length that was placed between the analyzed sample and the CPP. This way light passing through the sample is analyzed by the CPP which converts the output light to chromaticity according to the polarization function of the sample and the analyzed imaged is captured by the camera chip.

Figure 5a,b shows the pictures taken when different regions of the tissue, 350 μm apart, are imaged on the CPP device. The dashed area in both pictures is added to facilitate comparison

dx.doi.org/10.1021/nl204257g | Nano Lett. XXXX, XXX, XXX−XXX

of the region being imaged. The incident polarization of light was fixed for both images. It is seen that when the region above the dashed area is imaged through the CPP device the letters appear blue and background appears yellow (Figure 5a). On the other hand, when the bottom part of the dashed region is imaged through the CPP, the color contrast is switched and letters appear yellow and the background appear blue (Figure 5b). The results clearly demonstrate the ability of the CPP device to map the birefringence of a biological sample to color.

In Figure 5c,d, we demonstrate birefringence-contrast images of a plastic film obtained with a CPP device consisting of an array of dots (see Methods). The edge of the plastic film is in the center of the images. The images are obtained with the polarizer set to (c) 45° and (d) 57°. The ability of the CPP device to map birefringence to color contrast can be seen by comparing the left and right side of the images, as these represent transmission through air and plastic, respectively. The marked differences and the fact that the color contrast in the plastic side was eliminated when the polarizer was set to 57° give an excellent indication of the polarization rotation effect of the plastic film. It should be noted that light rotation in birefringent materials is wavelength-dependent, so calibrations and further calculations have to be performed to determine the value of the birefringence.

To show the advantage of the bright field polarization imaging enabled by CPPs, we imaged the birefringence of a plastic film with a conventional birefringence polarization measurement and compared to a measurement using CPP. The conventional way to measure birefringence of a sample is by placing it between two polarizers and analyzing the polarization functionality of the sample. In Figure 5e, we present the results obtained by placing the plastic sample between two 90° crossed Glan-Thompson polarizers and in Figure 5f when the input polarizer was rotated by 12°. Figure 5c,d shows the corresponding results obtained by placing the sample between one polarizer and one CPP when the polarizer was set to 45 and 57°, respectively. The top dark parts of Figure 5e,f were obtained with the same incident light intensity and the same image sensor brightness setting, β, as that used with the CPP device. It can be seen that the images captured with the polarizer pair are extremely dim compared to those obtained with the CPP device. The bottom parts of Figure 5e,f were obtained under identical conditions, except with the brightness increased 5-fold. The results obtained by the two methods agree where extinction of light or increased transmittance using the two crossed polarizers is equivalent to elimination of chromaticity or increased chromaticity respectively using the CPP. It can be seen that light extinction in air was better when the polarizers were crossed than when the input polarizer was rotated by 12°. On the other hand, for light passing through the plastic film, the extinction was better when the input polarizer was rotated by 12°. The blue color of light passing through the plastic is due to birefringence being inversely proportional to wavelength. Comparing Figure 5c,d with Figure 5e,f demonstrates the advantages of polarization imaging with CPP devices. The CPP devices give a bright-field indication of the polarization effects whereas crossed polarizer method is a dark-field technique and therefore requires higher intensities of light.

In this work, we realized CPPs based on aluminum ONATs that result in notch filtering of part of the transmitted visible spectrum. The color gamut accessible by notch filtering is limited, for example, it cannot be used to produce green color. However, it can be shown that CPPs can also be used as active visible band-pass filters by either relying on reflection from CPP ONATs or on the extraordinary transmission through unisotropic cross-shaped slits in metal. Another possibility that is not discussed in this work is to use CPPs as active dichroic devices that transform unpolarized light to chromatically polarized light at the output, for example, red and green beams that are cross polarized. Consequently, it can be used to produce polarization dependent colors where the analyzing polarizer sets the color of the beam.

In conclusion, we use in this work advances in nanotechnology to generate high-resolution, actively colored metasurfaces based on cross-shaped ONATs and show some of their unique applications. The polarization dependence of MNPs or metal cross apertures was well studied in the past.[2,4,11,15,19−23,30−32] However, here we take it a substantial step forward and demonstrate for the first time to our knowledge that such operation in the visible part of the spectrum can be mapped to continuous lines on the CIE 1931 chromaticity diagram that can be easily engineered and tuned and thus can be applied to a broad spectrum of interesting applications. These range from active color pixels for color display technology, to patterns whose appearance changes dramatically with polarization and therefore could form the basis for security tags, to devices for polarization imaging. The striking visible color effects make CPPs highly suitable for use with conventional color cameras or when viewed with the unaided eye. We are currently considering the extension of this concept to employ the magnetic resonances of nanostructures and to create novel types of three-dimensional colored metamaterials sensitive to both the polarization and angle of incident light.

■ ASSOCIATED CONTENT

Supporting Information

Methods, supplementary figures, supplementary movies, and supplementary discussions. This material is available free of charge via the Internet at http://pubs.acs.org.

■ AUTHOR INFORMATION

Corresponding Author

*E-mail: (T.E.) tale@seas.harvard.edu. Tel: +1-617-4952941. (K.B.C.) kcrozier@seas.harvard.edu. Tel: +1-617-4961441.

■ ACKNOWLEDGMENTS

This work was supported in part by the Center for Excitonics, an Energy Frontier Research Center funded by the U.S. Department of Energy, Office of Science and Office of Basic Energy Sciences under Award Number DE-SC0001088. The work was supported in part by Zena Technologies. Fabrication work was carried out in the Harvard Center for Nanoscale Systems (CNS), which is supported by the National Science Foundation.

■ REFERENCES

(1) Freeston, I.; Meeks, N.; Sax, M.; Higgitt, C. *Gold Bull.* **2007**, *40*, 270−277.
(2) Atwater, H.; Polman, A. *Nat. Mater.* **2010**, *9*, 205−213.
(3) Langhammer, C.; Schwind, M.; Kasemo, B.; Zoric, I. *Nano Lett.* **2008**, *8*, 1461−1471.
(4) Crozier, K. B.; Sundaramurthy, A.; Kino, G. S.; Quate, C. F. *J. Appl. Phys.* **2003**, *94*, 4632−4642.
(5) Schaadt, D. M.; Feng, B.; Yu, E. T. *Appl. Phys. Lett.* **2005**, *86*, 063106.

(6) Nakayama, K.; Tanabe, K.; Atwater, H. A. *Appl. Phys. Lett.* **2008**, *93*, 121904.
(7) Nie, S.; Emory, R. E. *Science* **1997**, *275*, 1102−1106.
(8) Talley, C. E.; Jackson, J. B.; Oubre, C.; Grady, N. K.; Hollars, C. W.; Lane, S. M.; Huser, T. R.; Nordlander, P; Halas, N. J. *Nano Lett.* **2005**, *5*, 1569−1574.
(9) Banaee, M. G.; Crozier, K. B. *Opt. Lett.* **2010**, *35*, 760−762.
(10) Chu, Y.; Banaee, M. G.; Crozier, K. B. *ACS Nano* **2010**, *4*, 2804.
(11) Zhu, W.; Banaee, M. G.; Wang, D.; Chu, Y.; Crozier., K. B. *Small* **2011**, *7*, 1761−1766.
(12) Hmanaka, Y.; Fukuta, K.; Nakamura, A.; Liz-Marzan, L. M. *Appl. Phys. Lett.* **2004**, *84*, 4938.
(13) Grady, N. K.; Halas, N. J.; Nordlander, P. *Chem. Phys. Lett.* **2004**, *399*, 167−171.
(14) Lal, S.; Link, S.; Halas, N. J. *Nat. Photonics* **2007**, *1*, 641−648.
(15) Bharadwaj, P.; Deutsch, B.; Novotny, L. *Adv. Opt. Photonics* **2009**, *1*, 438.
(16) Anker, J. N.; Hall, W. P.; Lyandres, O.; Shah, N. C.; Zhao, J.; Van Dyune, R. *Nat. Mater.* **2008**, *7*, 442−453.
(17) Chu, Y.; Schonbrun, E.; Yang, T.; Crozier, K. B. *Appl. Phys. Lett.* **2008**, *93*, 181108.
(18) Chu, Y.; Wang, D.; Zhu, W.; Crozier, K. B. *Opt. Express* **2011**, *19*, 14919−14928.
(19) Xu, T.; Wu, Y.; Luo, X.; Guo, J. *Nat. Commun.* **2010**, *1*, 59.
(20) Diest, K .; Dionne, J. A .; Spain, M .; Atwater, H. A . *Nano Lett.* **2009**, *9*, 2579−2583.
(21) Genet, C.; Ebbesen, T. W. *Nature* **2007**, *445*, 39−46.
(22) Lee, H. S.; Yoon, Y. T.; Lee, S. S.; Kim, S. H.; Lee, K. D. *Opt. Express* **2007**, *15*, 15457−15463.
(23) Laux, E.; Genet, C.; Skauli, T.; Ebbesen, T. W. *Nat. Photonics* **2008**, *2*, 161−164.
(24) Novotny, L. *Phys. Rev. Lett.* **2007**, *98*, 266802.
(25) Juan, M. L.; Righini, M.; Quidant, R. *Nat. Photonics* **2011**, *5*, 349−356.
(26) Wang, K.; Schonbrun, E.; Steinvurzel, P.; Crozier, K. B. *Nat. Commun.* **2011**, *2*, 469.
(27) Strasswimmer, J.; Pierce, M. C.; Park, B. H.; Neel, V.; de Boer, J. F. *J. Biomed. Opt.* **2004**, *9*, 292.
(28) Francis, R. C.; Carlson, D.; Blank, P. S. *Biophys. J.* **1989**, *56*, 401−413.
(29) Ellenbogen., T.; Polat, U.; Spitzer, H. *Spatial Vision* **2006**, *19*, 547−568.
(30) Lin, L.; Goh, X. M.; McGuinness, L. P.; Roberts, A. *Nano Lett.* **2010**, *10*, 1936−1940.
(31) Roth, M. R.; Panoiu, N. C.; Adams, M. M.; Dadap, J. I.; Osgood, M. *Opt. Lett.* **2007**, *32*, 3414−3416.
(32) Dirix, Y.; Bastiaansen, C.; Caseri, W.; Smith, P. *Adv. Mater.* **1999**, *11*, 223−227.

dx.doi.org/10.1021/nl204257g | *Nano Lett.* XXXX, XXX, XXX−XXX